Design and Characterization of Wideband Aperture-Coupled Circularly Polarized Antenna for Gigabits Per Second Wireless Communication System

Osama M. Haraz[1,2] · Muhammad A. Ashraf[3] · Nadeem Ashraf[3] · Saleh A. Alshebili[3]

Abstract

In this paper, design and characterization of an aperture-coupled circularly polarized (CP) rectangular patch antenna suitable for Gigabit per second wireless communications system is presented. The proposed antenna exhibits a large bandwidth of 2.77 GHz at centre frequency f_c = 19.5 GHz (about 15% of fractional bandwidth (FBW)). It also has a gain of about 7.25 dBi at 18 GHz with good stable gain and radiation characteristics in the frequency band of interest. For indoor wireless channel measurements, two developed prototypes are employed as single input single output transmit receive (TX–RX) antennas with a robust and versatile channel modeling system. We demonstrate a measurement campaign to investigate the dynamic range of the system by calculating path loss. The pulse dispersion effect is quantified by pulse fidelity factor (PFF). The measurements are performed in laboratory environment using Gaussian pulse based sounding signal modulated at 19.3 GHz carrier frequency. The design and characterization of compact size antennas with pertinent bandwidth and excellent radiation characteristics is one of our initiatives towards developing a millimeter wave (MMW) test bed system for channel modeling and measurement, since 5G wireless communication is supposed to operate in MMW band.

Keywords Circularly polarized antenna · Aperture-coupled antenna · Gigabits per second wireless system

✉ Osama M. Haraz
o_haraz@aun.edu.eg; o_haraz@su.edu.sa

1   Electrical Engineering Department, Faculty of Engineering, Assiut University, Assiut 71515, Egypt

2   Electrical Engineering Department, College of Engineering, Shaqra University, Dawadmi, Ar Riyadh 11911, Saudi Arabia

3   Technology Innovation Center in Radiofrequency and Photonics (RFTONICS) in the e-Society, King Saud University, Riyadh 11421, Saudi Arabia

1 Introduction

LAST few decades have witnessed massive research and technological innovations in the area of mobile communications. Comparing current advanced fourth-generation (4G) mobile communication with basic first-generation analog systems; we find a revolutionary improvement in the transmission rates of wireless data with a promise of excellent quality of service (QOS) [1–4]. Although the 4G network is aimed to offer data rates up to 1 Gb/s but the massive use of smartphones and video streaming applications have created demands more than several Gb/s. To support up to a thousand-fold increase in total mobile traffic by 2020, the untapped mm-wave frequency band is highly recommended for the next 5th generation wireless communication [5].

Due to the huge congestion of frequencies at the lower microwave spectrum, several research and development (R&D) activities have been performed to investigate the possible use of a higher order band (greater than 10 GHz) as a potential candidate for future wireless communication systems [6, 7]. Data transmission modulated with high-frequency carrier finds potential capability of achieving high-speed Gb/s communication since only a 10% fractional bandwidth at 20 GHz can provide data rate greater than 3 Gb/s. It has been manifested from many research activities and measurement campaigns found in the literature that antenna elements are considered as an important module to characterize important free space propagation parameters such as path loss, multipath delay spread and channel impulse response [6–10]. Several on-chip and antenna-in-package have been developed to be integrated with MMW wireless communication systems [11–14]. Despite the excellent characteristics of the developed state of the art antennas and individual antenna element should offer: (1) minimum return loss over the proposed spectrum, (2) minimum time dispersion for transmitting the pulse of desired bandwidth, (3) persistent radiation efficiency, (4) frequency independent radiation pattern and (5) compact size [15–17]. To ensure high-speed reliable data and video transmission, wideband antenna elements with excellent frequency and time domain characteristics are essential. Therefore, developing low profile high-frequency antennas satisfying all the above characteristics simultaneously is a hot topic of recent research.

A wideband data communication inherits dispersion due to various transmit and receive (TX–RX) active and passive components as well as the wireless channels. Therefore, it is important to characterize designed antenna elements with minimum dispersion. Generally, the dispersion effect of the antenna element is quantified by the pulse fidelity factor (PFF). To have a more realistic channel model, it is very important to include the PFF factor in the channel model, obtained by employing actual antennas in the system to be used.

In this communication, we present the design and fabrication of slot coupled circularly polarised antennas characterized for both time and frequency domain parameters. We demonstrate an exemplary time-domain measurement campaign of the indoor channel using 2 GHz bandwidth Gaussian pulse modulated at 19.3 GHz carrier from which dispersion effects of hardware components including antenna elements and path loss measurement to evaluate system dynamic range are reported. The presented work unifies: (i) design of aperture-coupled circularly polarized (CP) rectangular patch antenna element, (ii) designed antenna's frequency-domain characterization, (iii) channel's path loss measurements at proposed frequency. Design, implementation, and characterization of a multi-layered antenna are done using conventional PCB designing approach and state of the art measurement equipment, respectively. For generating and recording channel sounding signals, we proposed a testbed system that can be operated at mm-wave frequency up to 44 GHz

and 5 GHz sounding signal's bandwidth using vector signal generator (VSG) and arbitrary waveform generator (AWG), respectively. Due to certain limitations regarding measurement equipment, we performed our measurements at lower 19.3 GHz center frequency, since the electromagnetic wave's attenuation behavior at 19.3 GHz is found similar to 28 GHz and 38 GHz frequency band as shown in Fig. 1. We performed path loss measurements to find the system's dynamic range that is useful to select an appropriate separation between Tx and Rx antennas.

2 Antenna Element

2.1 Antenna Geometry and Design

The geometrical configuration of the antenna used for performing this experiment is shown in Fig. 2. The proposed antenna consists of an aperture-coupled circularly polarized (CP) rectangular patch antenna. The antenna consists of two different substrate materials; the upper one is Rogers® Duroid™ 5880 substrate with relative permittivity of 2.2 and loss tangent of 0.0009, while the lower one is Rogers® Duroid™ 6010 substrate with relative permittivity of 10.2 and loss tangent of 0.0023. On the top side of the upper substrate, there is a rectangular patch antenna.

The patch antenna that has a length L_P and width W_P, is chamfered by value D_P from its corners to achieve circular polarization. A common metallic ground plane separates the two substrates. A narrow rectangular slot with a length L_S and width W_S is etched from the ground plane for coupling purposes. On the other side of the lower substrate, there is a 50-Ω microstrip feedline of length L_f and width W_f. The coupling between the feedline and the patch has occurred via the slot in the middle ground plane. The proposed antenna was fabricated and the photographs of the fabricated prototype are shown in Fig. 2d. All optimized antenna parameters are summarized in Table 1.
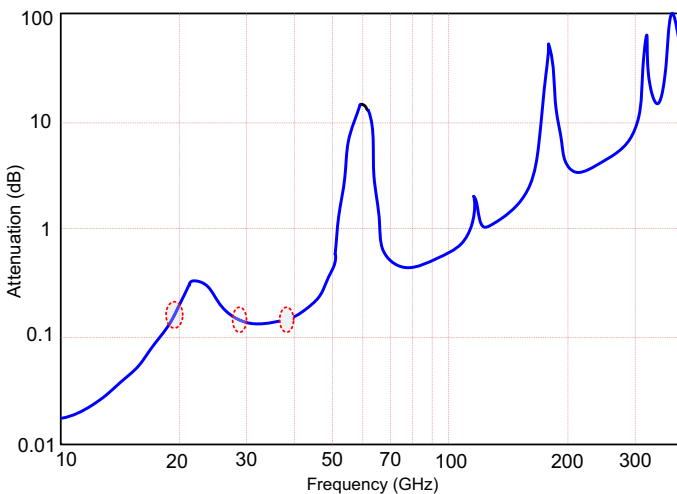

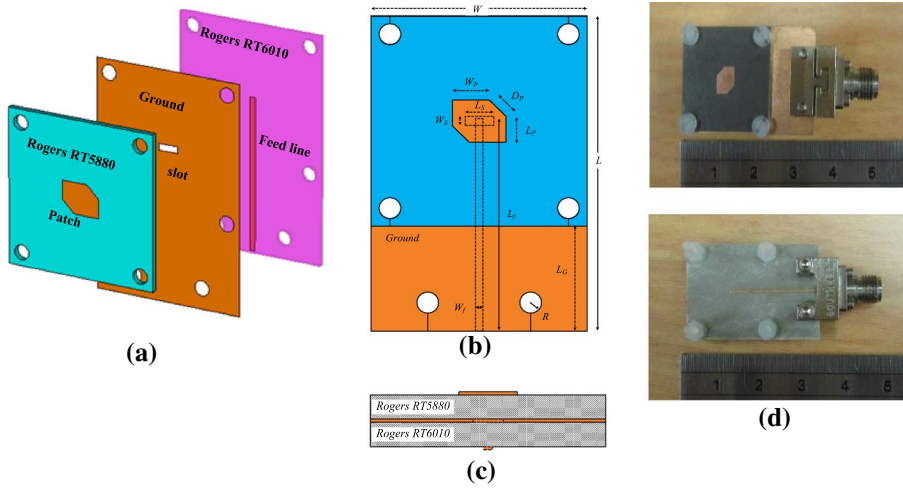**Fig. 1** Atmospheric absorption across mm-wave frequencies in dB/km [5]

Fig. 2 Geometrical configuration of proposed 5G antenna, **a** isometric view, **b** top view, **c** side view, and **d** photograph of fabricated prototype

Table 1 Optimized dimensions of the proposed antenna prototype (units in mm)

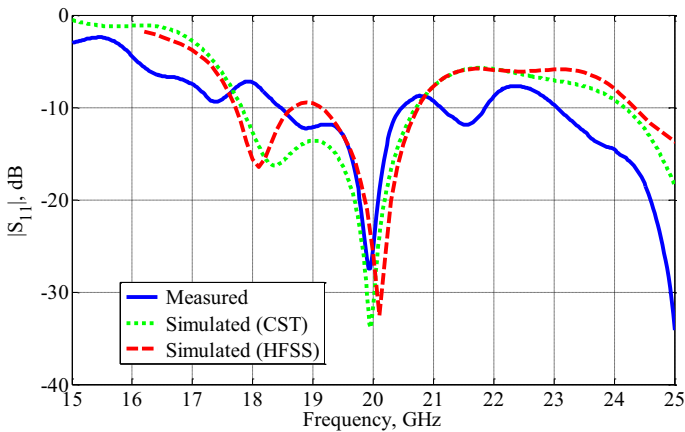| Parameter	W	L	W_P	L_P	D_P	W_S	L_S
Value	20	30	3.407	2.47	2.206	0.87	2.6
Parameter	W_f	L_f	R	L_G	H_1	H_2	
Value	0.738	20.2	1	10.03	0.787	0.787	

Fig. 3 Measured and simulated reflection coefficient $|S_{11}|$ versus frequency of the proposed antenna

2.2 Measured and Simulated Results

All simulations have been carried out using Computer Simulation Technology (CST) Microwave Studio software program [18]. Figure 3 presents the measured and simulated

reflection coefficient $|S_{11}|$ of the proposed antenna versus frequency. It can be seen that the antenna exhibits a large achieved simulated bandwidth of 2770 MHz at centre frequency f_c = 19.5 GHz (about 15% of fractional bandwidth (FBW)). The measured achieved impedance matching bandwidth is 2000 MHz from 18.5 to 20.5 GHz (about 10% of FBW). It is worthy to mention that the original antenna was designed to have a center frequency of 18 GHz and a bandwidth of 2000 MHz. After fabricating the antenna prototypes and due to the small air gaps between the two layers, it has been found that the antenna is operating at a higher frequency, i.e. 19.5 GHz instead of 18 GHz. This is due to lower the effective dielectric constant by introducing these air gaps and hence the centre frequency will be shifted up towards the higher frequencies. This explanation has been verified using CST full-wave simulation program.

For further understanding, the antenna operation, the antenna input impedance $Z = R + jX$ is calculated using CST MWS and plotted in Fig. 4. It can be seen that the real part of the antenna input impedance R is fluctuating around 50-Ω while the imaginary part jX is fluctuating around zero-Ω in the desired frequency range. It means that the antenna is well matched in the frequency range of interest.

The simulated electric field distributions of the proposed antenna at 18 GHz are calculated and presented in Fig. 5. The fields are calculated in all structure layers, i.e. top, middle, and bottom layers. This is to show the field distributions at feedline, coupling slot, and radiating patch. It can be noticed from the results that the proposed antenna exhibits a circular polarization. It can be seen that the electric field has been split into two equal magnitudes and orthogonal in-phase components. The three-dimensional (3D) radiation patterns of the proposed antenna have been simulated and presented in Fig. 6. The radiation patterns are calculated at three different frequencies 18, 19 and 20 GHz. A good radiation pattern stability is achieved across the frequency band of interest. Besides, antenna radiation patterns in both E- and H-planes at different frequencies, 18 GHz, 19 GHz, and 20 GHz are shown in Fig. 7.
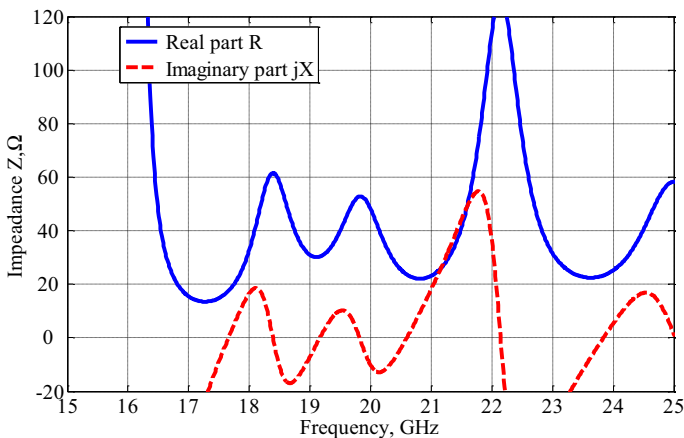

Fig. 4 Simulated antenna input impedance $Z = R + jX$ versus frequency of the proposed antenna

At upper layer   At middle layer   At lower layer
(patch)   (ground with   (feedline)
                        slot)
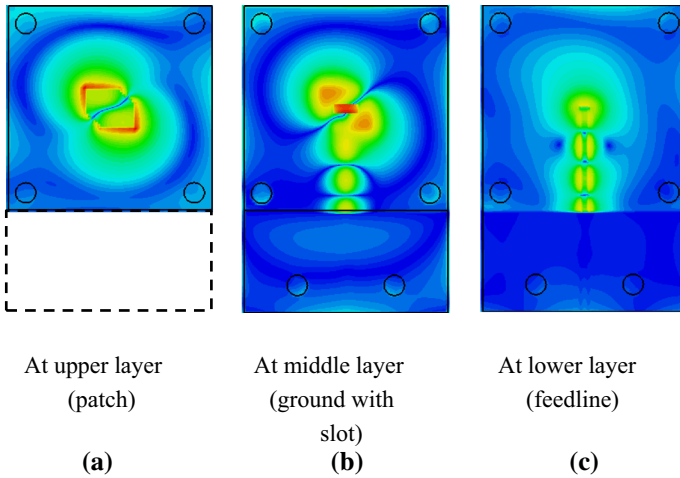(a)   (b)   (c)

Fig. 5 Simulated electric field distributions of the proposed antenna. **a** At upper layer (patch), **b** At middle layer (ground with slot), **c** At lower layer (feedline)
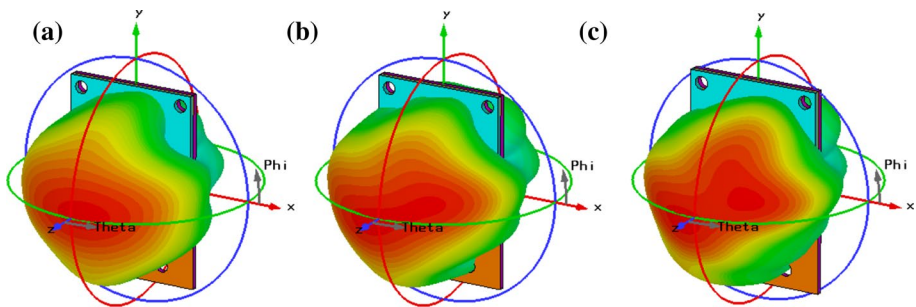

Fig. 6 Simulated 3D antenna radiation patterns of the proposed antenna at different frequencies **a** 18 GHz, **b** 19 GHz, and **c** 20 GHz

3 Path Loss Measurements

Path loss measurements are essential to design an indoor wireless communication system. The calculated link budget is found different from the measurements due to multipath propagations that are not constant for a particular indoor environment. The main purpose of these measurements is to find a particular distance between transmit and receive (Tx–Rx) antennas showing enough signal to noise ratio (SNR) that can be easily detected and processed by available receiver equipment. Figure 8 shows our proposed measurement system block diagram. The major equipment of the transmitter block contains Agilent Technologies Arbitrary Waveform Generator (AWG) M8190A 12 GSa/s, Vector Signal Generator (VSG) E8267D up to 44 GHz and in-house developed printed circuit board multi-layered antenna. We can set up complex signals of any arbitrary wave shape with effective bandwidth up to 5 GHz by using AWG. Two Digital to Analog (D/A) channels of AWG provide complex I/Q signals with programmable output voltage up to 1 Vp-p. The AWG's outputs are fed to broadband I/Q inputs of VSG that are available at the rare side of the equipment.
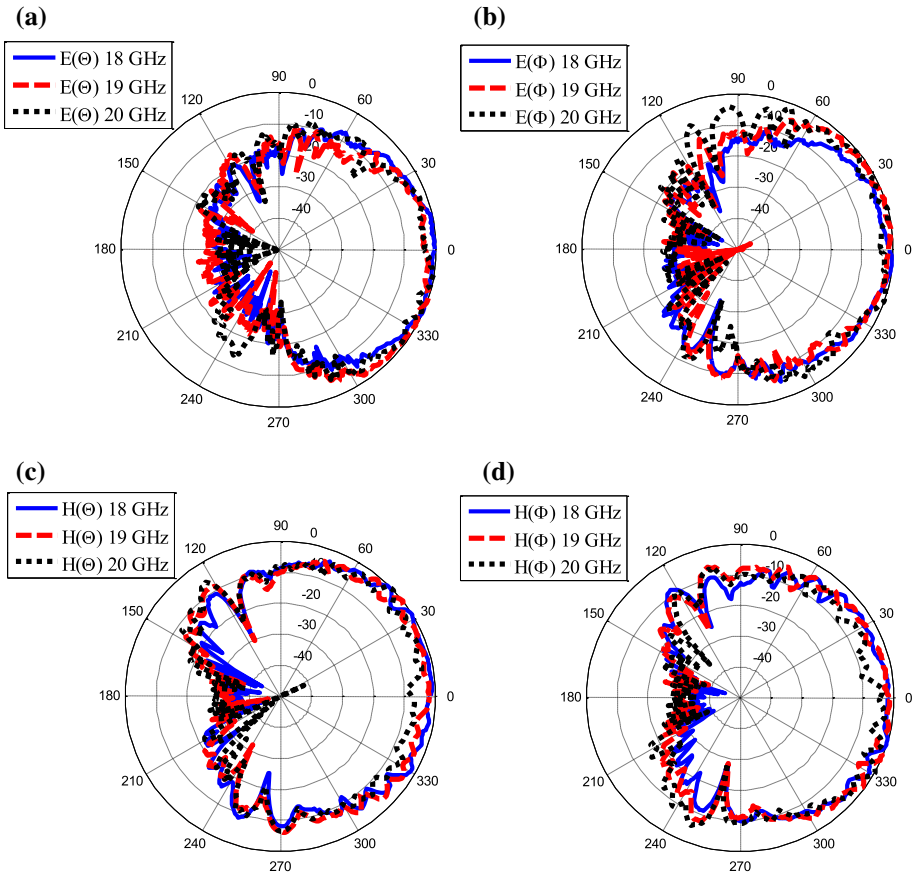
(a)

(b)

(c)

(d)

Fig. 7 Measured Co-pol and Cross-pol components of radiation pattern in **a** E-plane and **b** H-plane
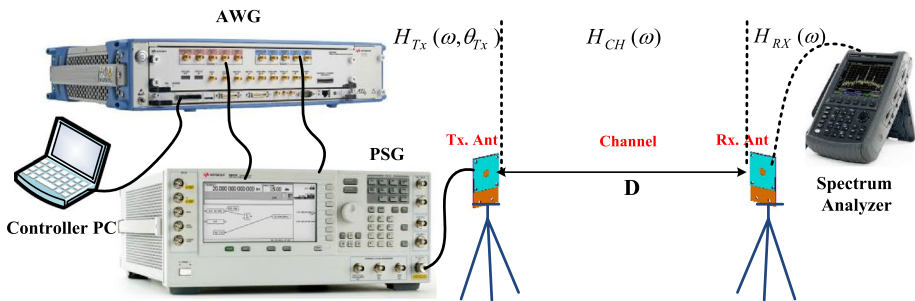

Fig. 8 Measurement system block diagram

The VSG's broadband mode can provide a maximum 2 GHz bandwidth with selectable output power and frequency steps up to 20 dBm (200 mW) and 44 GHz, respectively.

We organized our setup to perform channel propagation measurements at 28 GHz centre frequency that is a proposed band for 5th generation wireless communication, but due to

limitations in the operating frequency range of the receiver measurement equipment, we performed our measurements at 19.3 GHz centre frequency in an indoor lab environment. The receiver's equipment includes an antenna identical to the transmit side and a handheld microwave spectrum Analyser (HSA) N9938A of Agilent Technology.

The received signal is directly connected to HSA and channel propagation is studied for three different transmit and received antennas separations of 25 cm, 50 cm, and 100 cm, respectively. We measured path loss of carrier frequency at various separations of Rx–Tx antennas. We put them aligned to the study system's performance for line of sight (LOS) propagation as at high-frequency free space channel exhibits too much attenuation. To find path loss for a modulated signal, we generated a Gaussian pulse of 1.2 GHz bandwidth and modulated at proposed carrier frequency using AWG and VSG, respectively. We selected 20 dBm (100 mW) output power for both experiments. We didn't introduce any additional amplifier at either of transmitter or receiver antenna side as the maximum distance for different readings doesn't exceed than 1 m.

3.1 Analysis and Discussion

A simple path loss model is given by [6],

$$\overline{PL(d)[dB]} = PL(d_o)[dB] + 10n \log_{10}\left(\frac{d}{d_o}\right) \tag{1}$$

where the first terms present the path loss at a reference distance d_o and the second term presents path loss at relative distance d. The coefficient n presents the path loss exponent. The path loss exponent can vary due to various factors such as antenna types, layout environment, measurements system performance and height of Tx-Rx antennas, all of which could result in different values of the n. A comprehensive list of values for path loss exponent is depicted in the literature for the measurements done at different frequencies related to some typical indoor conditions. The values of n for indoor LOS propagation at 17 GHz and 21.6 GHz based measurements are found 1.2 and 1.16, respectively [19, 20]. For our current measurement at 19.3 GHz $n = 1.18$ could be an appropriate choice. To calculate $PL(d)[dB]$ according to (1), it is important to find path loss at reference distance (d_o). Typically, $d_o = 1$ m is used as the reference distance. Therefore, our objective in this experimental exercise is to measure path loss at the reference distance. Regarding the equipment used in our experimental measurement (see Fig. 9), we found the two identical antennas and interconnect cables have measured values of 7.75 dB gain and 3.5 dB loss, respectively. We calculated path loss by the following linear relationship

$$PL(d_o)[dB] = RSL_{mean} - P_{in} - 2G_{ant} + 2L_{cab} \tag{2}$$

where RSL, Pin, Gant, and Lcab stand for measured received signals level at HSA, input power transmitted by VSG, Tx–Rx antennas gain and interconnect cable losses, respectively. Figure 10 presents the amplitude received by HSA for the carrier ($f = 19.3$ GHz) and modulated Gaussian signals measured at three different Tx–Rx antennas separations. For carrier and modulated signal transmission at $D = 25$ cm (that is equal to 16λo in electrical wavelengths), the measured RSL is -35 dBm and -52.5 dBm, respectively. The calculated path loss values according to Eq. (2) are found 63.5 dB and 81 dB for carrier
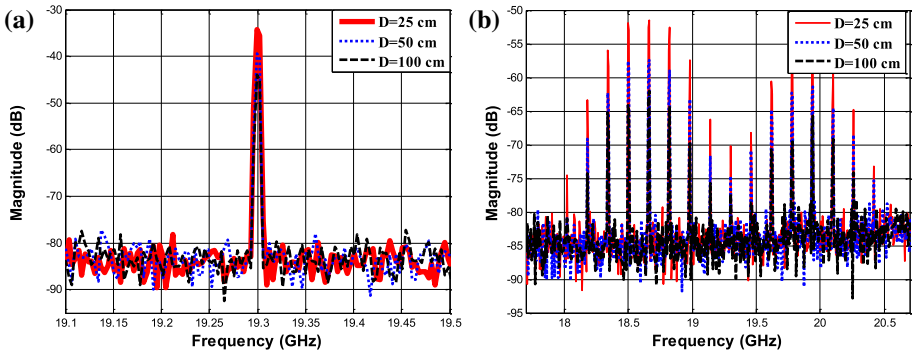
Fig. 9 Measured spectrum at different Tx–Rx aspirations **a** carrier frequency **b** modulated Gaussian
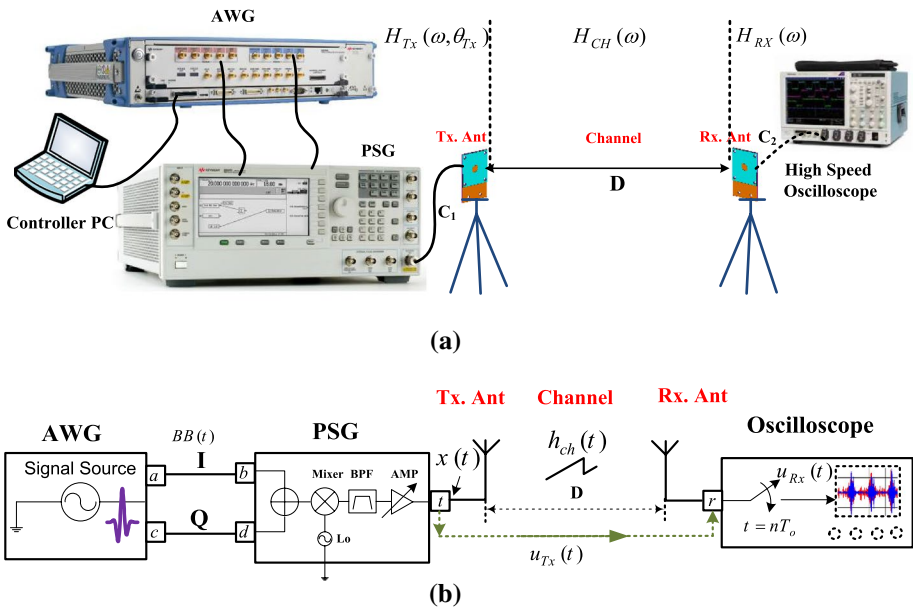

(a)

(b)

Fig. 10 Measurement setup **a** block diagram **b** equivalent functional blocks

and modulated signals, respectively. We also measured path loss at reference distance $do = 1$ m that can be used to find path loss for any arbitrary distance between Tx–Rx antennas.

4 High-Frequency Channel Modelling

Characterizing the antenna elements with free-space propagation of a wideband modulated signal at high-frequency is important for designing modern radio systems has been considered as a hot topic for current research. The block diagram portrayed in Fig. 10a presents a propagation measurement setup for any realistic sounding signal having bandwidth and

modulating carrier frequency up to 5 GHz and 44 GHz, respectively. As RF modulation bandwidth of VSG external I/Q input is 2 GHz maximum which limits the bandwidth of our sounding signal generated by AWG. The equivalent functional block diagram of the proposed measurement setup is shown in Fig. 10b. Compared to the measurement setup shown in Fig. 3 the HSA in the receiver block is replaced with 50 Gsa/s 20 GHz high speed mixed signal oscilloscope MSO72004C of Tektronix. In this scenario, we can measure and record received time-domain transmitted signals. In our proposed propagation measurement approach, sampling rate and sensitivity of the oscilloscope are significant parameters which define the maximum RF frequency range and the separation between Tx–Rx antennas, respectively. According to the Nyquist theorem, the sampling rate of digitizer should be twice ($Fs = 2 \times f_{Tx}$) than the maximum frequency of the signal to be analyzed in the digital domain. We performed our testing with 19.3 GHz carrier to have a modulated signal marginally below from 25 GHz maximum frequency limit. Similarly, to receive signal with a fair signal to noise ratio we chase $D = 50$ cm between Tx-Rx antennas which correspond to 32 λ_o at 19.3 GHz.

4.1 Radio Channel Model

We performed our measurements in Lab environment ensuring that the channel is stationary with no people moving around. Moreover, to avoid received signals from multi-paths, antennas are placed apart from nearby objects having 1 m height from the floor and in LOS condition. In this scenario, we assumed stationary and time-independent radio channels. However, we can't assume channel as frequency independent, since our sounding signal is modulated at high-frequency exhibits more than 10% fraction bandwidth. This is because the electromagnetic wave finds the attenuation proportional to 20log (frequency). Among the several sounding signals that can be used for channel probing are pseudo-noise (PN) sequence modulation, modulated Gaussian pulse, and frequency chirp modulation. In our measurements, a modulated Gaussian pulse is selected since it has the properties of maximum steepness of transition with minimum overshoots. The transmitted train of modulated Gaussian pulses is expressed as,

$$x(t) = BB(t) \cos(\omega_c t) \tag{3}$$

with

$$BB(t) = \sum_{k=1}^{n} \left(\alpha \sqrt{\pi} \right)^{-\frac{1}{2}} \left(e^{-\frac{t^2}{2\alpha^2}} - k\tau \right) \tag{4}$$

where α is the width controlling factor of the Gaussian pulse $u_{Tx}(t)$, τ is the pulse repetition time, n is the total number of pulses and $\omega_c/2\pi$ is the carrier frequency. The transmitted modulated Gaussian pulse has a nominal period of 6.2 ns. We set record length up to 31 ns resulting in five pulses in our observation window.

Consider $x(t)$ and $u_{RX}(t)$ be the transmitted and the received signals, respectively (see Fig. 11b). The model for free-space propagation in time-domain can be described as,

$$u_{RX}(t) = h_{Scope}(t) * h_{RXant}(t) * h_{CH}(t) * h_{TXant}(t) * x(t) \tag{5}$$
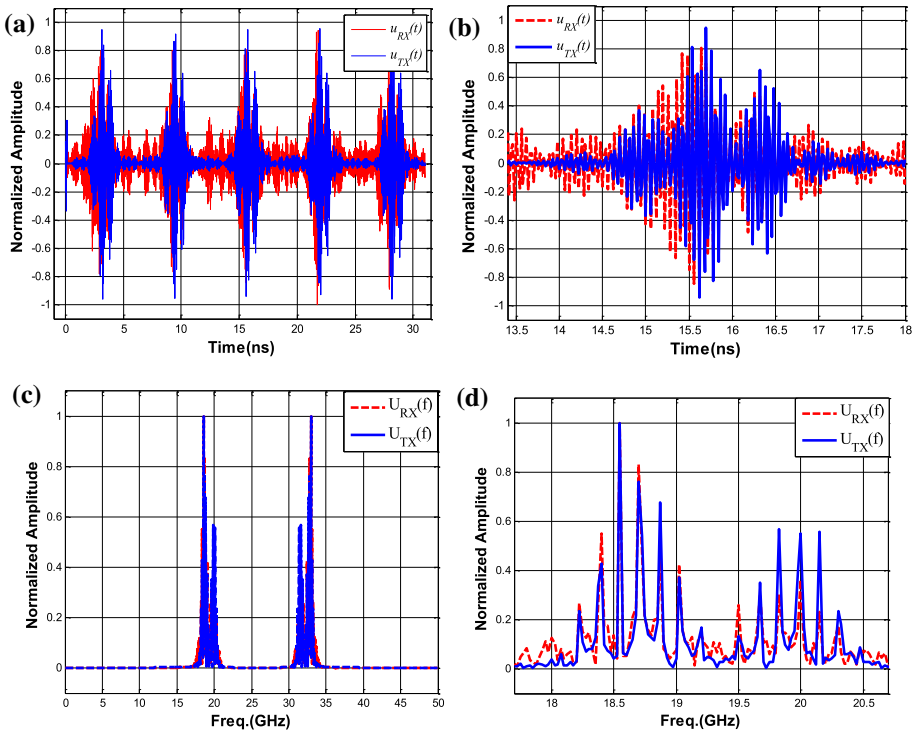
with

Fig. 11 Measured, **a**, **b** time domain modulated pulse trains for transmitted $u_{TX}(t)$ and received $u_{RX}(t)$ signals, **c**, **d** calculated spectrums

$$x(t) = h_{TX}(t) * BB(t) \tag{6}$$

where $h_{TX}(t)$ includes AWG and VSG characteristics, $h_{TXant}(t)$, $h_{RXant}(t)$, $h_{Scope}(t)$ and $h_{CH}(t)$ present Tx antenna, Rx antenna, oscilloscope and free space propagation characteristics, respectively. The equivalent frequency domain response can be written as,

$$U_{RX}(\omega) = H_{Scope}(\omega)H_{RXant}(\omega)H_{CH}(\omega)H_{TXant}(\omega)X(\omega) \tag{7}$$

with,

$$X(\omega) = H_{TX}(\omega)BB(\omega) \tag{8}$$

and

$$H_{sys}(\omega) = \frac{U_{RX}(\omega)}{X(\omega)} = H_{ScopeX}(\omega)H_{RXant}(\omega)H_{CH}(\omega)H_{TXant}(\omega) \tag{9}$$

where $H_{sys}(\omega)$ presents the response of the complete system including the components of transmitter and receiver blocks and the free space propagation channel. The transfer functions of the transmit and the receive antennas are reciprocal since both antennas are of the same type, $H_{TXant}(\omega) = H_{RXant}(\omega)$, resulting

$$H_{sys}(\omega) = \frac{U_{RX}(\omega)}{X(\omega)} = H_{Scope}(\omega)|H_{ant}(\omega)|^2 H_{CH}(\omega) \tag{10}$$

To record the transmitted signal $x(t)$, the output port of VSG is directly connected to the oscilloscope. In this case, the sounding signal is recorded without involving the Tx-Rx antennas and the wireless channel. Consider the recorded waveform $u_{TX}(t)$, which includes oscilloscope response that can be written as,

$$u_{TX}(t) = h_{Scope}(t)*x(t) \tag{11}$$

and

$$U_{TX}(\omega) = H_{Scope}(\omega)X(\omega) \tag{12}$$

According to (12) we can simplify (10) as,

$$H'_{sys}(\omega) = \frac{U_{RX}(\omega)}{U_{TX}(\omega)} = |H_{ant}(\omega)|^2 H_{CH}(\omega) \tag{13}$$

where H'_{sys} is the ratio of U_{RX} and U_{TX} which incorporates antennas and propagation channel responses.

4.2 Measurements and Signal Processing

Given the antenna element operating at 18.5–20.5 GHz band, we probed the propagation channel with a modulated pulse having carrier frequency centred at 19.3 GHz. Figure 11a presents normalized amplitude of both generated and received signals, recorded at 50 Gsa/s by connecting VSG output directly to the oscilloscope through a DC-26.5 GHz wideband coaxial cable and using Tx–Rx antenna via free-space propagation channel, respectively. The total record length is 31 ns presenting a sequence of five pulses. Figure 11b shows the.the zoomed version of the middle pulse portraying envelop of the modulated Gaussian pulse. The received signal is added with channel noise and dispersion effect caused by Tx–Rx antennas. Figure 11c displays the normalized spectrum of both signals calculated using MATLAB. The calculated spectrum shows reasonable agreement with the response measured by the spectrum analyzer shown in Fig. 10b.

The high-frequency components of the spectrum are lower in amplitude as compared to lower-frequency since channel exhibits more attenuation at a higher frequency. To stifle out-of-band noise, the received signal is passed through a band-pass Butterworth filter having order $n = 8$ and coefficients $W_n = 0.6821, 0.7974$ calculated at Fs/2. In passband, both signals seem similar showing good agreement, however, the amplitude of the received signal at different frequency components varies due to antennas and channel non-linear effects.

To compare the transmitted and received signals with the baseband Gaussian signal, the output waveform transmitted by AWG is also recorded using the oscilloscope. Bandpass to baseband conversion of the transmitted and the received signals is accomplished by synchronous digital down-conversion (amplitude demodulation) and Butterworth lowpass filter of the order $n = 6$. To have a fair comparison of demodulated signals with baseband, their waveforms are presented on the same graph as shown in Fig. 12a, b. The corresponding spectral representation is also presented in Fig. 12b, c. The portrayed signals find good agreement with each other except the signal received via free-space propagation
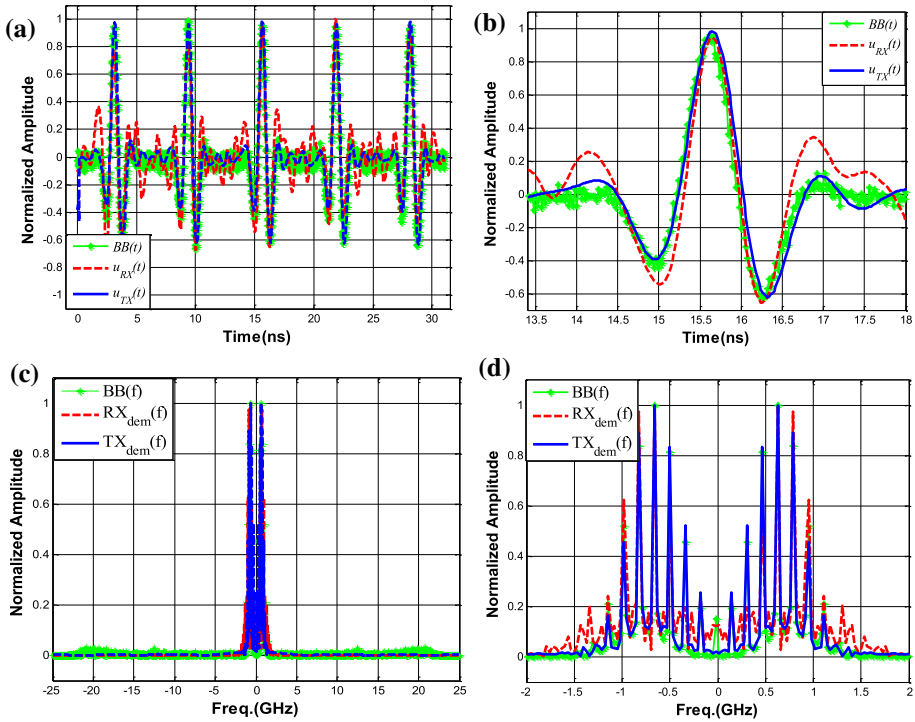
Fig. 12 Time domain measured **a**, **b** baseband signal $BB(t)$ and digitally demodulated received $u_{Rx}(t)$, transmitted $u_{Tx}(t)$ signals, **c**, **d** calculated spectrums

finds ringing and oscillation which implicates the addition of channel noise as well as non-linearities of antenna elements. We assumed stationary conditions of the channel, however, frequency dependency of the channel and the antenna elements causes received waveform deterioration. Moreover, in addition to the time and frequency domain characteristics, the special domain response of the antenna element also influences the Tx–Rx pulse shape. The preservation of pulse shape is quantified by the pulse fidelity factor (PFF). It gives us a value between zero and one showing the degree of mismatch between a reference and any arbitrary pulse. Ideally, the PFF value should be one. In our case, we consider BB(t) as a reference signal and $u_{Rx}(t)$ and $u_{Tx}(t)$ as arbitrary signals to find the PFF according to the following equation,

$$PFF = max_\tau \left| \frac{\int_{-\infty}^{+\infty} BB(t)u_{arb}(t-\tau)dt}{\sqrt{\int_{-\infty}^{+\infty}|BB|^2 dt \int_{-\infty}^{+\infty}|u_{arb}(t-\tau)|^2 dt}} \right|$$

where $BB(t)$ and $u_{arb}(t)$ stand for reference baseband and arbitrary signals, respectively. Replacing $u_{arb}(t)$ with $u_{Rx}(t)$ and $u_{Tx}(t)$, we find a strong correlation of these signals with $BB(t)$ resulting in PFF values 0.903 and 0.9842, respectively.

Based on our analysis, it is shown that the overall system offers a signal's deterioration that is not more than 10%. Moreover, it feasible to upgrade our proposed test-beds system

for indoor non-line of sight propagation channel measurements by introducing amplifiers at Tx–Rx blocks.

5 Conclusion

The design of a wireless channel propagation measurements and characterization setup capable of generating realistic-sounding signals operating in the MMW band is presented in this paper. We investigate path loss properties of the signal in a laboratory environment with perfect LOS conditions for antenna elements separated by 1 m, operating at 19.3 GHz frequency modulated with 2 GHz bandwidth Gaussian pulse that is found to be 81 dB. We designed, implemented and tested robust aperture coupled circularly polarized multi-layered patched antennas suitable for wideband data communication. The perceived dispersion effect caused by antenna elements and wideband propagation channels is less than 10% that is quantified by calculating PFF. Baseband conversion of high-frequency passband signal is accomplished using digital signal processing techniques. Our proposed setup will allow the researcher to investigate the solutions for technical challenges based on the use of, ultra-broad-bandwidth, waveform type mitigating current and future standards, multiple antennas and various channel sounders probing signals for next-generation wireless communication systems.

References

1. Shvidobadze, T. (2012). Evolution mobile wireless communication and LTE networks. In *2012 6th international conference on Application of information and communication technologies (AICT)* (pp. 1, 7).
2. Ku, G., &Walsh, J. (2015). Resource allocation and link adaptation in LTE and LTE advanced: A tutorial. *IEEE Communications Surveys & Tutorials*.
3. Viswanathan, H., & Weldon, M. (2014). The past, present, and future of mobile communications. *Bell Labs Technical Journal, 19,* 8–21.
4. Rappaport, T. S., et al. (2014). *Millimeter wave wireless communications*. Pearson Education.
5. Rangan, S., Rappaport, T. S., & Erkip, E. (2014). Millimeter-wave cellular wireless networks: Potentials and challenges. *Proceedings of the IEEE, 102*(3), 366–385.
6. Rappaport, T. S., Sun, S., Mayzus, R., Zhao, H., Azar, Y., Wang, K., et al. (2013). Millimeter wave mobile communications for 5G cellular: It will work! *IEEE Access, 1,* 335–349.
7. Kim, M., Konishi, Y., Chang, Y., & Takada, J.-I. (2014). Large scale parameters and double-directional characterization of indoor wideband radio multipath channels at 11 GHz. *IEEE Transactions on Antennas and Propagation, 62*(1), 430–441.
8. Hua, G., Yang, C., Lu, P., Zhou, H. X., & Hong, W. (2013). Microstrip folded dipole antenna for 35 GHz MMW communication. *International Journal of Antennas and Propagation*
9. Alhalabi, R. A., & Rebeiz, G. M. (2010). Differentially-fed millimeter-wave Yagi-Uda antennas with folded dipole feed. *IEEE Transactions on Antennas and Propagation, 58*(3), 966–969.
10. Gordon, G. S. D. (2013). *Design of indoor communication infrastructure for ultra-high capacity next generation wireless services*. Diss. University of Cambridge.
11. Bai, J., Shi, S., & Prather, D. W. (2011). Modified compact antipodal vivaldi antenna for 4–50-GHz UWB application. *IEEE Transactions on Microwave Theory and Techniques, 59*(4), 1051–1057.
12. Enayati, A., Vandenbosch, G. A. E., & Deraedt, W. (2013). Millimeter-wave horn-type antenna-in-package solution fabricated in a teflon-based multilayer PCB technology. *IEEE Transactions on Antennas and Propagation, 61*(4), 1581–1590.

13. Li, Y., & Luk, K.-M. (2014). Low-cost high-gain and broadband substrate-integrated-waveguide-fed patch antenna array for 60-GHz band. *IEEE Transactions on Antennas and Propagation, 62*(11), 5531–5538.
14. Cao, B., Wang, H., Huang, Y., Wang, J., & Xu, H. (2014). A novel antenna-in-package with LTCC technology for W-band application. *IEEE Antennas and Wireless Propagation Letters, 13*, 357–360.
15. Fujimoto, K., & Morishita, H. (2014). *Modern small antennas*. Cambridge: Cambridge University Press.
16. Santella, G. (1999). Analysis of antenna impact on wide-band indoor radio channel and measurement results at 1 GHz, 5.5 GHz, 10 GHz and 18 GHz. *Journal ofCommunications and Networks, 1*(3), 166–181.
17. Li, S., Yin, X., Wang, L., Zhao, H., Liu, L., & Zhang, M. (2014). Time-domain characterization of short-pulse networks and antennas using signal space method. *IEEE Transactions on Antennas and Propagation, 62*(4), 1862–1871.
18. CST Microwave Studio, Ver. (2015). *Computer Simulation Technology*. Framingham, MA, USA.
19. Rubio, M. L., Garcia-Armada, A., Torres, R. P., & Garcia, J. L. (2002). Channel modeling and characterization at 17 GHz for indoor broadband WLAN. *IEEE Journal on Selected Areas in Communications, 20*(3), 593–601.
20. Kalivas, G., El-Tanany, M., & Mahmoud, S. (1993). Channel characterization for indoor wireless communications at 21.6 GHz and 37.2 GHz. In *2nd international conference on universal personal communications, 1993. Personal communications: Gateway to the 21st century. Conference record* (Vol. 2, pp. 626–630).

Osama M. Haraz was born in Aswan, Egypt in October 23, 1976. He received the B.S. (with honors) and M.S. degree in electrical engineering from Assiut University, Egypt, in 1999 and 2004, respectively and the Ph.D. degree from Concordia University, Montreal, QC, Canada, in 2011. From 1999 to 2000 he worked with Nuclear Material Authority, Cairo, Egypt as an electronic engineer. Between 2000 and 2006 he was with the electrical engineering department of faculty of engineering, Assiut University as assistant lecturer. He is currently an Associate Professor of electrical engineering (Electronics & Communication Section), Assiut University. He is also working as Associate Professor at Electrical Engineering Department at College of Engineering at Shaqra University, Saudi Arabia. His current research interests include small antennas, microwave circuits for UWB and MMW applications, phased array antennas, interaction of EM waves with new advanced materials. Dr. Haraz received the 2010 Concordia Ph.D. thesis completion award, Concordia University, Montreal, Canada. He has also received the Scholarship of the Egyptian Ministry of Higher Education (2006–2010), the 2000 MobiNil communication company excellence award and the 6th October University Academic Distinction Award (1997–1998), Cairo, Egypt.

Muhammad A. Ashraf received the bachelor's degree in electrical engineering from the University of Engineering and Technology Lahore in 2003, the M.S. degree in microwave engineering from the National University of Sciences and Technology, Rawalpindi, in 2009, and the Ph.D. degree from King Saud University, Riyadh, in 2014. In 2003, he joined National Development Complex, a public sector organization. He joined the Telemetry Department and developed his expertise in the fields of electromagnetic wave propagation and S-band radio frequency (RF) front end components design. He was a Lecturer with the National University of Computer and Emerging Sciences from 2007 to 2008. In 2008, he joined the Electrical Engineering Department, King Saud University. During his Ph.D. research, he was with the Microwave, Antenna and Radar Systems Laboratory, Prince Sultan Advanced Technology Research Institute, King Saud University. He is currently with the Technology Innovation Center, RF and Photonics for the e-Society, funded by King Abdulaziz City for Science and Technology.

Nadeem Ashraf Department of Electrical and Computer Engineering Concordia University Montreal, QC, H3G 2W1, Canada

Saleh A. Alshebili a Professor, and Chairman of Electrical Engineering Department at King Saud University. He received the B.Sc. and M.Sc. Degrees in Electrical Engineering from King Saud University in 1984 and 1986, respectively. He received the Ph.D. degree in Electrical Engineering from University of Toronto, Ontario, Canada, in 1992. His research interests are in the area of Signal Processing with Applications to Communications, Speech, and Image Processing.